Comprehensive magnetohydrodynamic hybrid simulations of fast ion driven instabilities in a Large Helical Device experiment

Y. Todo, R. Seki, D. A. Spong, et al.

ARTICLES YOU MAY BE INTERESTED IN

Linear and nonlinear particle-magnetohydrodynamic simulations of the toroidal Alfvén eigenmode
Physics of Plasmas **5**, 1321 (1998); https://doi.org/10.1063/1.872791

Basic physics of Alfvén instabilities driven by energetic particles in toroidally confined plasmas
Physics of Plasmas **15**, 055501 (2008); https://doi.org/10.1063/1.2838239

Properties of energetic-particle continuum modes destabilized by energetic ions with beam-like velocity distributions
Physics of Plasmas **13**, 082503 (2006); https://doi.org/10.1063/1.2234296

Comprehensive magnetohydrodynamic hybrid simulations of fast ion driven instabilities in a Large Helical Device experiment

Y. Todo,[1,2,a)] R. Seki,[1,2] D. A. Spong,[3] H. Wang,[1] Y. Suzuki,[1,2] S. Yamamoto,[4] N. Nakajima,[1] and M. Osakabe[1,2]

[1]*National Institute for Fusion Science, Toki, Gifu 509-5292, Japan*
[2]*Department of Fusion Science, SOKENDAI (The Graduate University for Advanced Studies), Toki, Gifu 509-5292, Japan*
[3]*Oak Ridge National Laboratory, Oak Ridge, Tennessee 37831, USA*
[4]*Institute of Advanced Energy, Kyoto University, Uji, Kyoto 611-0011, Japan*

Alfvén eigenmodes (AEs) destabilized by the neutral beam injection (NBI) in a Large Helical Device experiment are investigated using multi-phase magnetohydrodynamic (MHD) hybrid simulation, which is a combination of classical and MHD hybrid simulations for fast ions. The fast ion distribution is simulated with NBI, collisions, and losses in the equilibrium magnetic field in the classical simulation, while the MHD hybrid simulation takes account of the interaction between fast ions and an MHD fluid, in addition to the classical dynamics. It is found in the multi-phase hybrid simulation that the stored fast ion energy is saturated due to the interaction with AEs at a lower level than that of the classical simulation. Two groups of AEs with frequencies close to those observed in the experiment are destabilized alternately at each hybrid simulation. Firstly destabilized are two toroidal Alfvén eigenmodes whose frequency is close to the local minimum of the upper Alfvén continuous spectrum. Secondly destabilized is a global Alfvén eigenmode whose frequency is located well inside the Alfvén continuous spectrum gap. In addition, two AEs whose frequencies are close to that of the ellipticity-induced Alfvén eigenmode are observed with a lower amplitude. When the hybrid simulation is run continuously, the interchange mode grows more slowly than the AEs, but becomes dominant in the long time scale. The interchange mode oscillates with a constant amplitude and a frequency of ∼1 kHz. The interchange mode reduces the stored fast ion energy to a lower level than that of the AEs. *Published by AIP Publishing.* [http://dx.doi.org/10.1063/1.4997529]

I. INTRODUCTION

Fast ions created by the neutral beam injection (NBI) and the ion-cyclotron-range-of-frequency (ICRF) wave have the important function of heating the bulk plasma in magnetic confinement fusion. In burning plasmas, alpha particles born from the deuterium and tritium (D-T) reaction are expected to heat the plasma to maintain the high temperature that is required for the D-T reaction. The fast ions can resonate with Alfvén eigenmodes (AEs) in the collisional slowing-down process, and may destabilize and amplify the AEs. The fast ion transport by the amplified AEs flattens the fast ion spatial profile and leads to fast ion losses. The interaction between fast ions and AEs is an important research subject for tokamak and stellarator/heliotron plasmas.[1–3]

Computer simulation is a powerful tool to investigate the interaction between fast ions and AEs. The multi-phase magnetohydrodynamic (MHD) hybrid simulation, which is a combination of classical simulation and MHD hybrid simulation, has been developed to investigate the fast ion distribution formation process with the interaction of the MHD instabilities in the collisional time scale.[4] The multi-phase hybrid simulations were successfully validated with the DIII-D experiment on the significantly flattened fast ion

pressure profile and the electron temperature fluctuations brought about by the AEs.[5] Alfvén eigenmodes have been studied extensively not only in tokamak plasmas but also in stellarator/heliotron plasmas.[6–13] In this work, we apply the multi-phase MHD hybrid simulation to the Large Helical Device (LHD) experiment #47645 (Ref. 8) and compare the simulation results with the experiment. In the LHD experiment, recurrent AE bursts were observed with two major peaks in the frequency spectrum at $t \sim 0.58$ s. The first peak in the frequency spectrum appears at $f = 50$–60 kHz, and the second peak appears alternately at $f = 65$–70 kHz in the burst duration shorter than 1 ms. The hole and clump structures were found in the fast ion velocity space distribution with the Neutral Particle Analyzer (NPA) on a LHD.[8] The hole and clump structures are formed in recurrent AE bursts. The fast ion radial transport over 10% of the minor radius was inferred by comparing the slowing-down time between the hole and the clump.

The AEs observed in the LHD experiment were analyzed using the AE3D code,[14] and even and odd toroidal Alfvén eigenmodes (TAEs) were found for the candidates for the AEs at the bursts.[15] Reduced simulations, where the spatial profiles and the frequencies of the AEs are given by the AE3D code and fixed in the simulations, demonstrate that the AE bursts take place recurrently with neutral beam injection (NBI) and collisions.[16,17] The amplitude of the

a)todo@nifs.ac.jp

MHD velocity v and the magnetic fluctuation δB that is consistent with the beam ion transport over 10% of the minor radius were investigated and found to be of the order of $v/v_A \sim \delta B/B \sim 10^{-3}$, where v_A and B are the Alfvén velocity and the magnetic field at the plasma center, respectively.[15,17] The AEs in the LHD plasma have been recently analyzed with the gyrokinetic particle code GTC.[18] In this work, we investigate the AEs in the experiment with the multi-phase hybrid MHD simulation, and also the fast ion redistribution brought about by the AEs. In addition, we find that an interchange mode becomes dominant with a constant amplitude and a low frequency $f \sim 1$ kHz when we run the MHD hybrid simulation continuously.

II. SIMULATION MODEL

A. MHD hybrid simulation model for energetic particles

We use the MEGA code,[19] in which the bulk plasma is described by the nonlinear MHD equations and the energetic ions are simulated with the gyrokinetic particle-in-cell (PIC) method. Several hybrid simulation models have been constructed[19–25] to study the evolution of Alfvén eigenmodes destabilized by energetic particles. An extended MHD model given in Ref. 26 has been implemented together with the equilibrium toroidal flow in MEGA.[5,27] In this paper, we use the standard MHD equations with the energetic ion effects

$$\frac{\partial \rho}{\partial t} = -\nabla \cdot (\rho \mathbf{v}) + \nu_n \triangle (\rho - \rho_{eq}), \tag{1}$$

$$\rho \frac{\partial}{\partial t} \mathbf{v} = -\rho \mathbf{v} \cdot \nabla \mathbf{v} - \nabla p$$
$$+ (\mathbf{j} - \mathbf{j}'_h) \times \mathbf{B} + \frac{4}{3} \nabla (\nu \rho \nabla \cdot \mathbf{v}) - \nabla \times (\nu \rho \boldsymbol{\omega}), \tag{2}$$

$$\frac{\partial p}{\partial t} = -\nabla \cdot (p\mathbf{v}) - (\gamma - 1)p\nabla \cdot \mathbf{v}$$
$$+ (\gamma - 1)\left[\nu \rho \omega^2 + \frac{4}{3}\nu\rho(\nabla \cdot \mathbf{v})^2 + \eta \mathbf{j} \cdot (\mathbf{j} - \mathbf{j}_{eq}) \right]$$
$$+ \chi \triangle (p - p_{eq}), \tag{3}$$

$$\frac{\partial \mathbf{B}}{\partial t} = -\nabla \times \mathbf{E}, \quad \mathbf{j} = \frac{1}{\mu_0} \nabla \times \mathbf{B}, \tag{4}$$

$$\mathbf{E} = -\mathbf{v} \times \mathbf{B} + \eta(\mathbf{j} - \mathbf{j}_{eq}), \tag{5}$$

$$\boldsymbol{\omega} = \nabla \times \mathbf{v}, \tag{6}$$

where μ_0 is the vacuum magnetic permeability, $\gamma = 5/3$ is the adiabatic constant, and ν, ν_n and χ are artificial viscosity and diffusion coefficients chosen to maintain numerical stability. In this work, the dissipation coefficients ν, ν_n, χ, and η/μ_0 are assumed to be equal to each other. The dissipation terms play a physical role in enhancing the damping of AEs in the MHD simulation that does not include kinetic damping such as radiative damping[28] and thermal ion Landau damping. In this paper, we use one value of the coefficients, 5×10^{-7}, normalized by $v_A R_0$, where v_A is the Alfvén velocity at the plasma center and R_0 is the major radius at the geometrical center of the simulation domain. The subscript "eq"

represents the equilibrium variables. The MHD momentum equation [Eq. (2)] includes the energetic ion contribution in the energetic ion current density $\mathbf{j}'_h$ that consists of the contributions from parallel velocity, magnetic curvature and gradient drifts, and magnetization current. The $\mathbf{E} \times \mathbf{B}$ drift disappears in $\mathbf{j}'_h$ due to quasi-neutrality.[19] We see that the electromagnetic field is given by the standard MHD description. This model is accurate under the condition that the energetic ion density is much less than the bulk plasma density. The MHD equations are solved using a fourth order (in both space and time) finite difference scheme.

The energetic ions are simulated using the full-f particle-in-cell (PIC) method, and a guiding-center approximation,[29] where we employ the gyrokinetic approach to account for finite Larmor radius (FLR) effects. The electromagnetic fluctuations are averaged over the energetic ion gyro orbit for the energetic ion dynamics (gyro-phase averaging).[30] However, the gyro-phase averaging is turned off in the simulations presented in this paper. The equations of motion for each computational particle are solved using a fourth-order Runge-Kutta method. The MEGA code participated in the code benchmark of the Energetic Particle Physics Topical Group of the International Tokamak Physics Activity.[31] Good agreement was found regarding the spatial profile, the frequency, and the growth rate of a TAE among the 7 codes without the energetic ion FLR effects and among the 6 codes with the FLR effects. The MHD part of the MEGA code is the same as the MIPS code, which shows good agreement with the CAS3D code in the ballooning modes in the LHD.[32,33]

B. Equilibrium, beam injection, collisions and losses

We try to simulate the LHD experiment #47645 at $t = 0.58$ s. The equilibrium data are constructed with the HINT code.[34,35] The magnetic field at the plasma center is $B_0 = 0.62$ T, and the major radius is $R_{\text{axis}} = 3.75$ m. Cylindrical coordinates (R, φ, z) are used for the HINT equilibrium and the simulations. For the purpose of data analysis, Boozer coordinates[36] (r, ζ, ϑ) are constructed for the MHD equilibrium, where r is the radial coordinate with $r = 0$ at the plasma center and $r = a$ at the plasma edge, and ζ and ϑ are the toroidal and poloidal angles, respectively. The profiles of rotational transform, electron density, electron temperature, and drag rate (inverse of the slowing-down time of beam ions) are shown in Fig. 1. We notice that the electron density has the hollow profile which increases from the center to the edge. Both the bulk and beam ions are hydrogen.

In the LHD experiment, three tangential neutral beams were injected.[8] As the magnetic field direction was reversed, two beams were found to be co-going to the effective plasma current, and one beam was counter-going. The three beams have injection energies of 181 keV, 160 keV, and 169 keV, respectively. The beam injection power was 4.5 MW, 2.6 MW, and 2.8 MW, respectively. In this work, we assume that the injection power of each beam is equally 3.0 MW. We employ the beam deposition profile calculated with the HFREYA code.[37] For the total beam injection power of
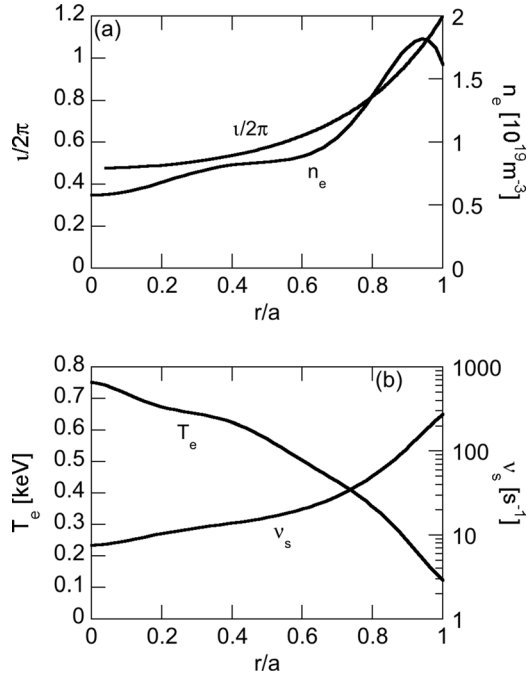
FIG. 1. Radial profiles of (a) rotational transform, electron density, (b) electron temperature, and drag rate (inverse of the slowing-down time).

9.0 MW, the HFREYA code gives the beam deposition power of 5.0 MW.

The numbers of grid points are (128, 640, 128) for (R, φ, z) coordinates, respectively, and the number of computational particles is 2.1×10^7. It was confirmed in a reduced simulation of bursting evolution of five AEs with the toroidal mode number $n = 1-5$ that 2 million particles are sufficient for numerical convergence in the burst interval, modulation depth of the stored fast ion energy at each burst, and saturation level of the stored fast ion energy.[38] Good convergence was also found with the similar number of particles per cell for the AEs and the energetic particle redistributions in an ITER plasma.[39] The reason why the relatively small number of particles works well may be that the phase space of energetic particles can be efficiently covered by the computational particles when we apply PIC only to the energetic particles and not to thermal particles. Another reason for the hybrid simulation with full MHD is that the time step width is limited by the Courant condition for a fast magnetosonic wave. This may reduce the effective numerical noise for AEs because the energetic particle distribution is computed more frequently.

Collisions of energetic ions with thermal electrons and ions[40] are implemented in the MEGA code. The slowing-down is included in the time integration of total particle velocity v by

$$\left(\frac{dv}{dt}\right)_{\text{slowing down}} = -\nu_s\left(v + \frac{v_c^3}{v^2}\right), \quad (7)$$

where ν_s is the drag rate (inverse of the slowing-down time) and v_c is the critical velocity above which the energetic ion collisions with electrons dominating the slowing-down process. Pitch-angle scattering and energy diffusion are taken

into account at the end of each time step using a Monte Carlo procedure,[41] where a particle's pitch λ and the total velocity v are altered according to the relations

$$\lambda_{\text{new}} = \lambda_{\text{old}}(1 - 2\nu_d\Delta t) \pm \left[(1 - \lambda_{\text{old}}^2)2\nu_d\Delta t\right]^{1/2}, \quad (8)$$

$$v_{\text{new}} = v_{\text{old}} + \frac{\nu_s\Delta t}{m_h v_{\text{old}}}\left[T_e - \frac{1}{2}T_i\left(\frac{v_c}{v_{\text{old}}}\right)^3\right]$$

$$\pm \left\{\frac{\nu_s\Delta t}{m_h}\left[T_e + T_i\left(\frac{v_c}{v_{\text{old}}}\right)^3\right]\right\}^{1/2}, \quad (9)$$

where ν_d is the pitch-angle scattering rate, m_h is the energetic ion mass, Δt is the time step width, T_e, T_i are, respectively, electron and ion temperature, and $\pm$ denotes a randomly chosen sign with an equal probability for plus and minus. We performed a classical simulation using the MEGA code for the MHD equilibrium and the beam deposition profile and compared the fast ion distribution with that simulated with the MORH code.[42] We found good agreement for the velocity space distribution and the fast ion pressure profile between the two codes.[43]

C. Multi-phase simulation

We would like to investigate the energetic ion distribution formation process with beam injection, collisions, losses, and transport due to the AEs. A complicating factor is that the time scale of the classical processes without MHD perturbations is the slowing-down time, which is roughly $\sim$100 ms, and longer by four orders of magnitude than the typical oscillation period of AEs $\sim$0.01 ms. The time step width is limited by the Courant condition for fast magnetosonic waves in the hybrid simulation. On the other hand, in the classical simulation, where the MHD part of the simulation is turned off, the time step width can be taken to be greater by one order of magnitude than in the hybrid simulation. To deal with this efficiently, a multi-phase simulation, where the classical simulation and the hybrid simulation are run alternately, was constructed.[4] In the classical phase of the simulation, the energetic ion distribution is built up with the beam injection and collisions. In the subsequent hybrid phase, the built-up energetic ion distribution destabilizes AEs leading to the relaxation of the distribution. We should note that the classical processes, beam injection and collisions, also take place in the hybrid phase. We repeat this combination of the classical and hybrid simulations until the stored energetic ion energy is saturated.

III. SIMULATION RESULTS

We performed multi-phase MHD hybrid simulations alternating the classical phase for 4 ms and the hybrid phase for 2 ms until the stored energetic ion energy is saturated. The time step widths for the classical phase and the hybrid phase are 5 ns and 1.7 ns, respectively. The time step width for the classical phase is relatively short compared with that in the tokamak simulations, because the grid size in the toroidal direction is small for the simulations in the LHD
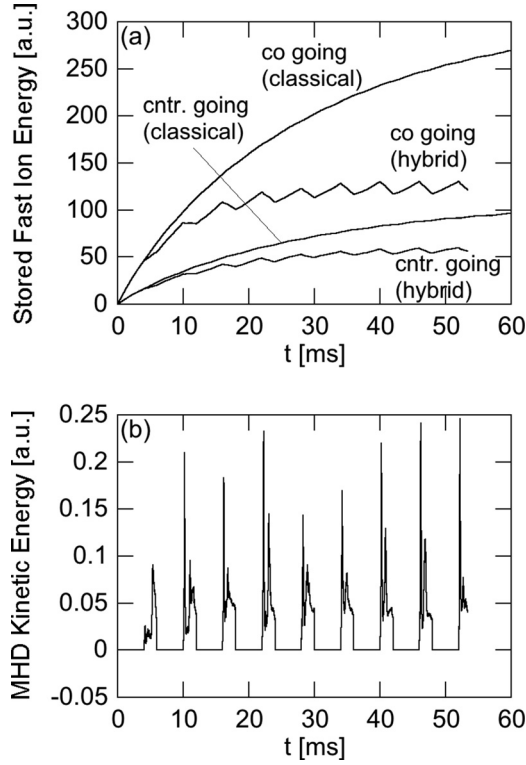
FIG. 2. Time evolutions of (a) stored fast ion energy in classical and multi-phase MHD hybrid simulations and (b) MHD kinetic energy in the multi-phase MHD hybrid simulation.

equilibrium which is twisted 10 times in the toroidal direction. Computational particles are injected at a constant rate over a beam injection period $t_{inj} = 100$ ms. In the LHD experiment #47645, the AEs observed have a toroidal mode number $n = 1$. We restrict the fast ion current density $\mathbf{j}'_h$ in Eq. (2) to have only the modes of $n = 1$ family ($n = 1, 9, 11, 19, 21, \ldots$) to focus on the $n = 1$ modes destabilized by fast ions.

A. Global Alfvén eigenmode (GAE) and TAEs

The time evolution of stored fast ion energy and that of MHD kinetic energy are shown in Fig. 2. We see in Fig. 2(a) that the stored fast ion energy is saturated at lower levels in the multi-phase MHD hybrid simulation. Figure 3 shows the frequency spectra of the radial MHD velocity fluctuation at $r/a = 0.68$ for poloidal and toroidal mode numbers
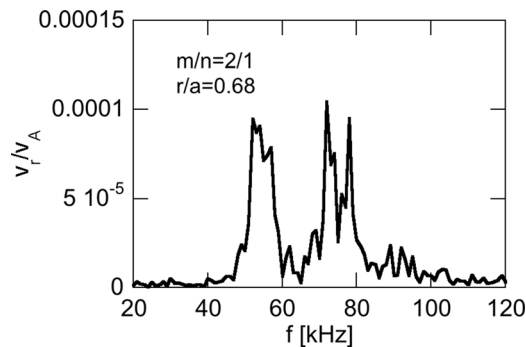

FIG. 3. Frequency spectrum of radial MHD velocity fluctuation at $r/a = 0.68$ for 34 ms $\leq t \leq 36$ ms. The mode number is $m/n = 2/1$.

$m/n = 2/1$ for 34 ms $\leq t \leq 36$ ms. The dominant peaks are $f = 52$ kHz, $f = 72$ kHz, and $f = 78$ kHz. The spatial profile with each peak frequency is shown in Fig. 4. The frequency and the location are shown for each mode with the Alfvén continuous spectra for the major toroidal harmonic $n = 1$ and $n = 11$ in Fig. 5. The Alfvén continuous spectra were analyzed with the STELLGAP code.[44] The mode with $f = 52$ kHz, whose spatial profile is shown in Fig. 4(a), has only one dominant poloidal harmonic $m = 2$. The frequency is located well inside the spectrum gap, but is separated from the TAE gap for $\iota/2\pi = 2/3$ at $r/a = 0.64$. This mode can be classified as a global Alfvén eigenmode (GAE). The modes with $f = 72$ kHz and $= 78$ kHz shown in Figs. 4(b) and 4(c) have two dominant poloidal harmonics $m = 1$ and 2. They are located around the TAE gap at $r/a = 0.64$. The frequencies are close to the upper continuous spectrum, and the sign of the $m = 1$ harmonic is opposite to the $m = 2$ harmonic. These are the properties of odd TAE.[45] These modes are classified as TAEs.

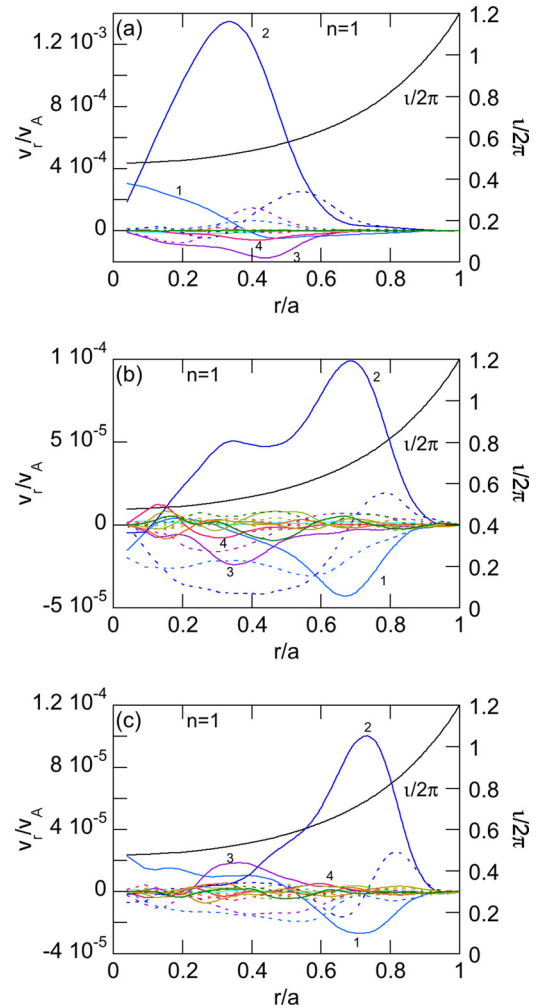The time evolution of the radial MHD velocity fluctuations at $r/a = 0.34$ and 0.73 is shown in Fig. 6. The

FIG. 4. Spatial profiles of radial MHD velocity fluctuation for 34 ms $\leq t \leq 36$ ms with toroidal mode number $n = 1$ and frequency (a) $f = 52$ kHz, (b) $f = 72$ kHz, and (c) $f = 78$ kHz. Solid (dashed) lines show $\cos(m\theta + n\zeta)$ [$\sin(m\theta + n\zeta)$] harmonics with the poloidal mode number m labelled in the figure.
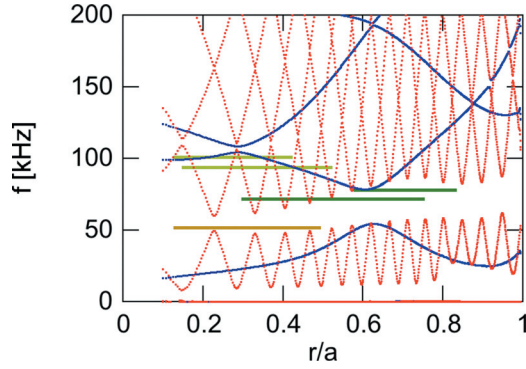
FIG. 5. Alfvén continuous spectra of the toroidal mode number (a) $n = 1$ (blue) and (b) $n = 11$ (red). The frequency and the spatial location of each AE with frequency $f = 52, 72, 78, 94, 101$ kHz are shown with a horizontal line.

fluctuation at $r/a = 0.34$ belongs mainly to the GAE with $f = 52$ kHz, and the fluctuation at $r/a = 0.73$ is mainly the TAEs with $f = 72$ kHz and $f = 78$ kHz. We see that the TAEs with $f \sim 75$ kHz at $r/a = 0.73$ grow earlier in Fig. 6(b), and the GAE with $f = 52$ kHz at $r/a = 0.34$ appears later in 6(a). Such an alternate appearance of two frequency ranges was observed in the LHD experiment #47645 [Fig. 9(d) of Ref. 8]. In the experiment, the mode with $f = 50$–60 kHz appears earlier, and the mode with $f = 65$–70 kHz appears later. Two frequency ranges appear alternately in both the simulation and the experiment, whereas the order of appearance is different. The maximum amplitude is $v_r/v_A \sim 2$–3×10^{-3} for both the fluctuations, which is comparable to those inferred for the fast ion transport suggested by the NPA measurement.[15,17] The fast ion pressure profiles are compared between before and after the AE burst in Fig. 7.
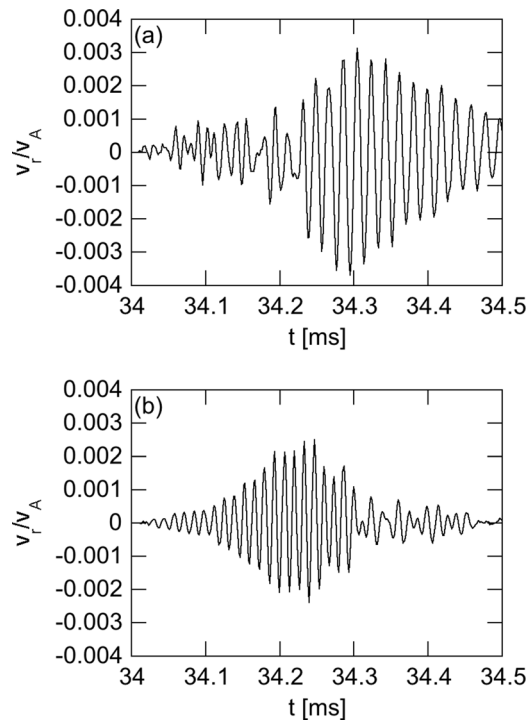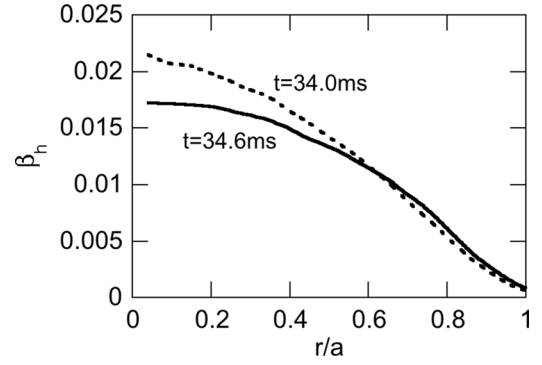

FIG. 7. Comparison of fast ion beta profiles at $t = 34.0$ ms (dashed line) and 34.6 ms (solid line).

We see that the fast ion profile is flattened and reduced at $r/a \leq 0.6$.

B. Modes close to the ellipticity-induced Alfvén eigenmode (EAE) gap

In addition to the GAE and TAEs, modes with frequency ~ 100 kHz close to the ellipticity-induced gap are found. The frequency and the location of the modes are shown in Fig. 5. Figure 8 displays the spatial profiles. The mode with $f = 94$ kHz shown in Fig. 8(a) has two dominant poloidal harmonics $m = 1$ and 3. The coupling between poloidal harmonics m and $m + 2$ is the property of ellipticity-induced Alfvén eigenmode (EAE). However, since the frequency is located below the upper continuous spectrum, this mode might be classified as a GAE. The other mode with $f = 101$ kHz shown in Fig. 8(b) also has two dominant
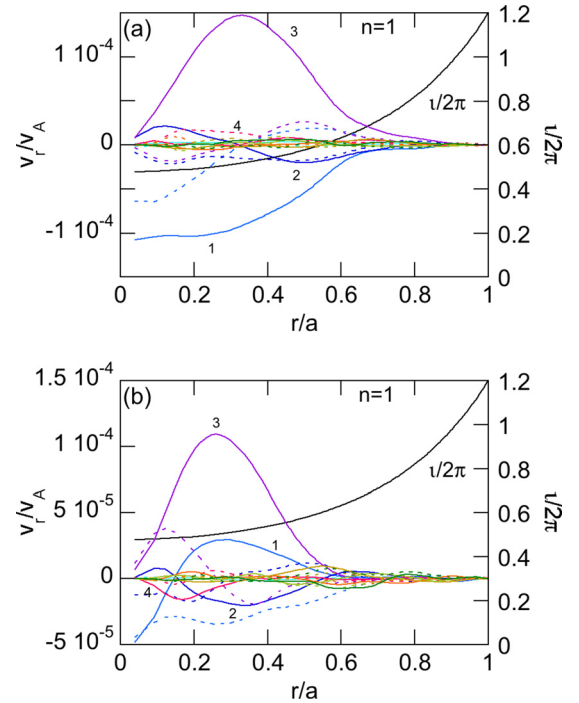

FIG. 6. Time evolution of radial MHD velocity fluctuations with $m/n = 2/1$ at (a) $r/a = 0.34$ and (b) $r/a = 0.73$ for 34 ms $\leq t \leq 34.5$ ms.

FIG. 8. Spatial profiles of radial MHD velocity fluctuations for 34 ms $\leq t \leq 36$ ms with the toroidal mode number $n = 1$ and frequency (a) $f = 94$ kHz and (b) $f = 101$ kHz. Solid (dashed) lines show $\cos(m\theta + n\zeta)$ [$\sin(m\theta + n\zeta)$] harmonics with the poloidal mode number m labelled in the figure.
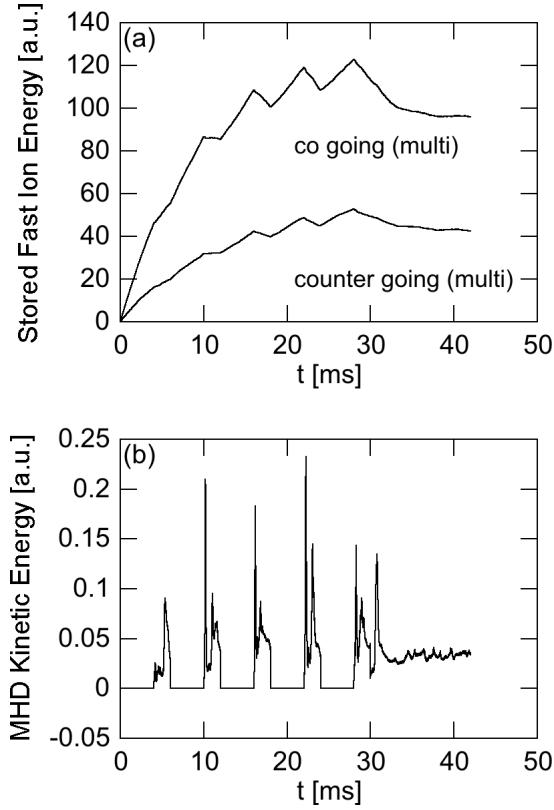
FIG. 9. Time evolutions of (a) stored fast ion energy and (b) MHD kinetic energy for the multi-phase MHD hybrid simulation where the hybrid simulation is continuously run after $t = 30$ ms.

poloidal harmonics $m = 1$ and 3. This mode might be an EAE, although the frequency is located slightly lower than the EAE gap in Fig. 5.

C. Continuous hybrid simulation

In our previous multi-phase MHD hybrid simulations for tokamak plasmas, we ran the hybrid simulation continuously at the end of the simulation and confirmed that the AE amplitudes reach steady levels or the AE bursts take place recurrently. For the simulation presented in Secs. III A and III B, we have run the hybrid simulation continuously for $t \geq$ 30 ms. The time evolution of stored fast ion energy and that of MHD kinetic energy are shown in Fig. 9. We see in Fig. 9(a) that the stored fast ion energy decreases for $t \geq 30$ ms and reaches lower levels than in the multi-phase simulation shown in Fig. 2(a). We do not see any burst in the MHD kinetic energy after the first increase at $t = 30$ ms in Fig. 9(b). The dominant mode for $t \geq 30$ ms is not the AEs discussed in Secs. III A and III B, and is the interchange instability. The MHD equilibrium we employed for this work is unstable for the interchange instability. Figure 10 shows the spatial profiles of radial MHD velocity fluctuation and radial magnetic fluctuation of the interchange instability that is analyzed by an MHD simulation where no fast ion is considered. The growth rate of the interchange instability is $5.5 \times 10^{-3} v_A / R_{axis}$. The interchange mode grows more slowly than the AEs, but becomes dominant in the continuous hybrid simulation.
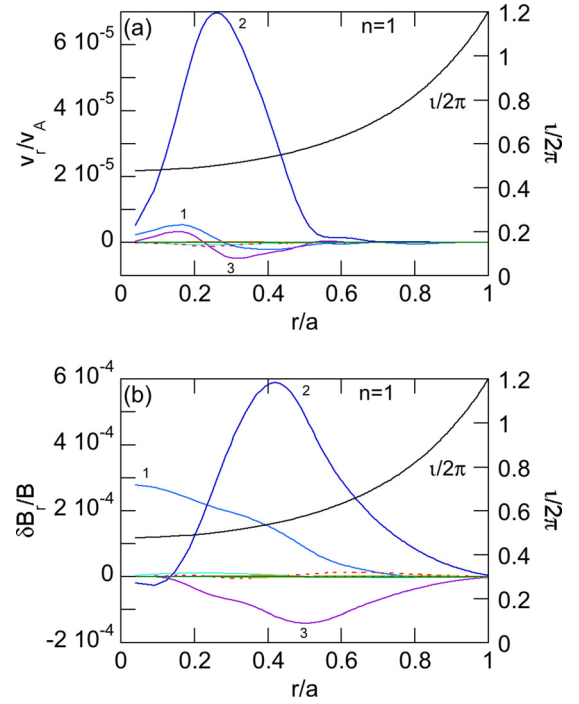

FIG. 10. Spatial profiles of (a) radial MHD velocity fluctuation and (b) radial magnetic fluctuation for the $n = 1$ interchange mode with the poloidal mode number m labelled in the figure.

Figure 11 shows the spatial profile of the radial magnetic fluctuation at $t = 42$ ms and the time evolution of the $m/n = 1/1$ harmonic at the peak location. We see that the mode is oscillating with a constant amplitude and a frequency of ~ 1 kHz. Without fast ions, the frequency of the interchange mode is 0. The significant reduction in stored fast ion energy
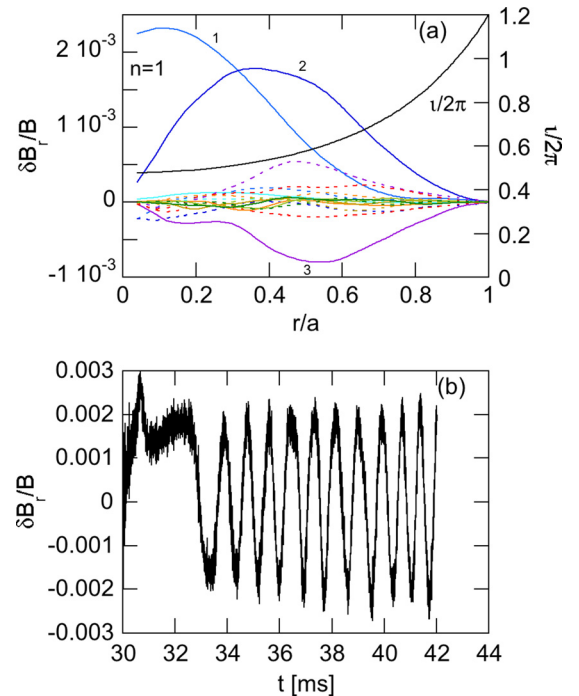

FIG. 11. (a) Spatial profile of radial magnetic fluctuation at $t = 42$ ms and (b) time evolution of $m/n = 1/1$ harmonics of radial magnetic fluctuation at the peak location.

after $t = 30$ ms shown in Fig. 9 is brought about by the interaction with the interchange mode. The finite frequency and the reduction in the stored fast ion energy indicate the interaction of the interchange mode with fast ions.

IV. SUMMARY AND DISCUSSION

We investigated AEs destabilized by the NBI in an LHD experiment with the multi-phase MHD hybrid simulation, which is a combination of classical and MHD hybrid simulations for fast ions. In the classical simulation, the fast ion distribution is simulated with NBI, collisions, and losses in the equilibrium magnetic field. The MHD hybrid simulation takes account of the interaction between fast ions and an MHD fluid in addition to the classical dynamics. It was found in the multi-phase hybrid simulation that the stored fast ion energy is saturated due to the interaction with AEs at a lower level than that of the classical simulation. Two groups of AEs with frequencies close to those observed in the experiment are destabilized alternately at each hybrid simulation. Firstly destabilized are two TAEs whose frequency is close to the local minimum of the upper Alfvén continuous spectrum. Secondly destabilized is a GAE whose frequency is located well inside the Alfvén continuous spectrum gap. Such an alternate appearance of two frequency ranges was observed in the LHD experiment #47645.[8] Two frequency ranges appear alternately in both the simulation and the experiment, whereas the order of appearance is different. The maximum amplitude is $v_r/v_A \sim 2 - 3 \times 10^{-3}$ for both the fluctuations in the simulation, which is also comparable to those inferred for the fast ion transport suggested by the NPA measurement.[15,17] The fast ion pressure profile is flattened at $r/a \leq 0.6$ at each AE burst. In addition, two EAE-like modes were observed with a lower amplitude. When the hybrid simulation is run continuously, an interchange mode grows more slowly than the AEs, but it becomes dominant in the long time scale. The interchange mode oscillates with a constant amplitude and a frequency of ~ 1 kHz. The interchange mode reduces the stored fast ion energy to a lower level than the AEs.

We would like to point out two interesting research subjects that are suggested by the simulation results in this paper. The first subject is the GAE whose frequency is well inside the Alfén continuous spectrum gap. The frequency of Aflvén eigenmodes is, in general, close to an extremum of the continuous spectrum. It is interesting to note that the frequency of the GAE is close to the extrema of the $n = 11$ continuous spectrum, as is shown in Fig. 5. Although the $n = 11$ harmonics of the GAE is negligibly small compared with the dominant $m/n = 2/1$ harmonic, the GAE seems to avoid the continuum damping with the $n = 11$ harmonics. It would also be important to investigate the non-perturbative effect of energetic particles on the properties of the GAE.[46,47] The second subject is the interaction between energetic particles and the interchange mode. Though the interchange mode is not observed in the particular LHD experiment #47645, energetic-particle driven interchange modes have been observed in the LHD.[48] In the simulation results presented in this paper, the interchange mode oscillates with a constant amplitude and frequency $f \sim 1$ kHz for a long time of ~ 9 ms. The interchange mode with the constant amplitude looks similar to the long lived modes observed in tokamak plasmas.[49] The interaction between the energetic particles and the interchange mode for both the linear and nonlinear regimes should be carefully examined in the near future.

[1]K. Toi, K. Ogawa, M. Isobe, M. Osakabe, D. A. Spong, and Y. Todo, Plasma Phys. Controlled Fusion **53**, 024008 (2011).
[2]S. Sharapov, B. Alper, H. Berk, D. Borba, B. Breizman, C. Challis, I. Classen, E. Edlund, J. Eriksson, A. Fasoli, E. Fredrickson, G. Fu, M. Garcia-Munoz, T. Gassner, K. Ghantous, V. Goloborodko, N. Gorelenkov, M. Gryaznevich, S. Hacquin, W. Heidbrink, C. Hellesen, V. Kiptily, G. Kramer, P. Lauber, M. Lilley, M. Lisak, F. Nabais, R. Nazikian, R. Nyqvist, M. Osakabe, C. P. von Thun, S. Pinches, M. Podesta, M. Porkolab, K. Shinohara, K. Schoepf, Y. Todo, K. Toi, M. V. Zeeland, I. Voitsekhovich, R. White, V. Yavorskij, ITPA EP TG, and JET-EFDA Contributors, Nucl. Fusion **53**, 104022 (2013).
[3]N. Gorelenkov, S. Pinches, and K. Toi, Nucl. Fusion **54**, 125001 (2014).
[4]Y. Todo, M. A. Van Zeeland, A. Bierwage, and W. Heidbrink, Nucl. Fusion **54**, 104012 (2014).
[5]Y. Todo, M. A. Van Zeeland, A. Bierwage, W. Heidbrink, and M. Austin, Nucl. Fusion **55**, 073020 (2015).
[6]A. Weller, D. A. Spong, R. Jaenicke, A. Lazaros, F. P. Penningsfeld, and S. Sattler, Phys. Rev. Lett. **72**, 1220 (1994).
[7]S. Yamamoto, K. Toi, N. Nakajima, S. Ohdachi, S. Sakakibara, K. Y. Watanabe, M. Goto, K. Ikeda, O. Kaneko, K. Kawahata, S. Masuzaki, T. Morisaki, S. Morita, S. Murakami, K. Narihara, Y. Oka, M. Osakabe, Y. Takeiri, K. Tanaka, T. Tokuzawa, K. Tsumori, H. Yamada, I. Yamada, and K. Yamazaki (LHD Experimental Group), Phys. Rev. Lett. **91**, 245001 (2003).
[8]M. Osakabe, S. Yamamoto, K. Toi, Y. Takeiri, S. Sakakibara, K. Nagaoka, K. Tanaka, and K. Narihara, and LHD Experimental Group. Nucl. Fusion **46**, S911 (2006).
[9]M. Isobe, K. Toi, K. Goto, C. Suzuki, K. Nagaoka, N. Nakajima, S. Yamamoto, S. Murakami, A. Shimizu, Y. Yoshimura, T. Akiyama, T. Minami, M. Nishiura, S. Nishimura, D. S. Darrow, D. A. Spong, K. Shinohara, M. Sasao, K. Matsuoka, and S. Okamura, and CHS Team, Nucl. Fusion **46**, S918 (2006).
[10]K. Nagaoka, M. Isobe, K. Toi, A. Shimizu, A. Fujisawa, S. Ohshima, H. Nakano, M. Osakabe, Y. Todo, T. Akiyama, Y. Nagashima, C. Suzuki, S. Nishimura, Y. Yoshimura, K. Matsuoka, and S. Okamura, Phys. Rev. Lett. **100**, 065005 (2008).
[11]K. Toi, F. Watanabe, T. Tokuzawa, K. Ida, S. Morita, T. Ido, A. Shimizu, M. Isobe, K. Ogawa, D. A. Spong, Y. Todo, T. Watari, S. Ohdachi, S. Sakakibara, S. Yamamoto, S. Inagaki, K. Narihara, M. Osakabe, K. Nagaoka, Y. Narushima, K. Y. Watanabe, H. Funaba, M. Goto, K. Ikeda, T. Ito, O. Kaneko, S. Kubo, S. Murakami, T. Minami, J. Miyazawa, Y. Nagayama, M. Nishiura, Y. Oka, R. Sakamoto, T. Shimozuma, Y. Takeiri, K. Tanaka, K. Tsumori, I. Yamada, M. Yoshinuma, K. Kawahata, and A. Komori (LHD Experiment Group), Phys. Rev. Lett. **105**, 145003 (2010).
[12]K. Ogawa, M. Isobe, K. Toi, F. Watanabe, D. A. Spong, A. Shimizu, M. Osakabe, S. Ohdachi, S. Sakakibara, and LHD Experiment Group. Nucl. Fusion **50**, 084005 (2010).

[13] R. Jiménez-Gómez, A. Könies, E. Ascasíbar, F. Castejón, T. Estrada, L. G. Eliseev, A. V. Melnikov, J. Jiménez, D. G. Pretty, D. Jiménez-Rey, M. Pedrosa, A. de Bustos, and S. Yamamoto, Nucl. Fusion **51**, 033001 (2011).

[14] D. A. Spong, E. D'Azevedo, and Y. Todo, Phys. Plasmas **17**, 022106 (2010).

[15] Y. Todo, N. Nakajima, M. Osakabe, S. Yamamoto, and D. A. Spong, Plasma Fusion Res. **3**, S1074 (2008).

[16] Y. Todo, S. Murakami, T. Yamamoto, A. Fukuyama, D. A. Spong, S. Yamamoto, M. Osakabe, and N. Nakajima, Fusion Sci. Technol. **58**, 277 (2010).

[17] S. Nishimura, Y. Todo, D. A. Spong, Y. Suzuki, and N. Nakajima, Plasma Fusion Res. **8**, 2403090 (2013).

[18] D. A. Spong, I. Holod, Y. Todo, and M. Osakabe, Nuclear Fusion **57**, 086018 (2017).

[19] Y. Todo and T. Sato, Phys. Plasmas **5**, 1321 (1998).

[20] W. Park, S. Parker, H. Biglari, M. Chance, L. Chen, C. Z. Cheng, T. S. Hahm, W. W. Lee, R. Kulsrud, D. Monticello, L. Sugiyama, and R. White, Phys. Fluids B: Plasma Phys. **4**, 2033 (1992).

[21] D. A. Spong, B. A. Carreras, and C. L. Hedrick, Phys. Fluids B: Plasma Phys. **4**, 3316 (1992).

[22] Y. Todo, T. Sato, K. Watanabe, T. H. Watanabe, and R. Horiuchi, Phys. Plasmas **2**, 2711 (1995).

[23] S. Briguglio, G. Vlad, F. Zonca, and C. Kar, Phys. Plasmas **2**, 3711 (1995).

[24] G. Y. Fu, W. Park, H. R. Strauss, J. Breslau, J. Chen, S. Jardin, and L. E. Sugiyama, Phys. Plasmas **13**, 052517 (2006).

[25] X. Wang, F. Zonca, and L. Chen, Plasma Phys. Controlled Fusion **52**, 115005 (2010).

[26] R. D. Hazeltine and J. D. Meiss, *Plasma Confinement* (Addison-Wesley Publishing Company, 1992).

[27] Y. Todo, M. A. Van Zeeland, and W. Heidbrink, Nucl. Fusion **56**, 112008 (2016).

[28] R. R. Mett and S. M. Mahajan, Phys. Fluids B: Plasma Phys. **4**, 2885 (1992).

[29] R. G. Littlejohn, J. Plasma Phys. **29**, 111 (1983).

[30] W. Lee, J. Comput. Phys. **72**, 243 (1987).

[31] A. Könies, S. Briguglio, N. Gorelenkov, T. Fehér, M. Isaev, P. Lauber, A. Mishchenko, D. A. Spong, Y. Todo, W. A. Cooper, R. Hatzky, R. Kleiber, M. Borchardt, G. Vlad, and I. E. TG, in Proceedings of the 24th International Conference on Fusion Energy (San Diego, 2012) ITR/P1-34 (IAEA, 2012).

[32] Y. Todo, N. Nakajima, M. Sato, and H. Miura, Plasma Fusion Res. **5**, S2062 (2010).

[33] C. Nührenberg, Phys. Plasmas **6**, 137 (1999).

[34] K. Harafuji, T. Hayashi, and T. Sato, J. Comput. Phys. **81**, 169 (1989).

[35] Y. Suzuki, N. Nakajima, K. Watanabe, Y. Nakamura, and T. Hayashi, Nucl. Fusion **46**, L19 (2006).

[36] A. H. Boozer, Phys. Fluids **26**, 1288 (1983).

[37] S. Murakami, N. Nakajima, and M. Okamoto, Trans. Fusion Technol. **27**, 256 (1995).

[38] Y. Todo, H. L. Berk, and B. N. Breizman, Phys. Plasmas **10**, 2888 (2003).

[39] Y. Todo and A. Bierwage, Plasma Fusion Res. **9**, 3403068 (2014).

[40] W. Heidbrink and G. Sadler, Nucl. Fusion **34**, 535 (1994).

[41] A. H. Boozer and G. KuoPetravic, Phys. Fluids **24**, 851 (1981).

[42] R. Seki, Y. Matsumoto, Y. Suzuki, K. Y. Watanabe, K. Hamamatsu, and M. Itagaki, Plasma Fusion Res. **5**, 027 (2010).

[43] R. Seki, Y. Todo, Y. Suzuki, and M. Osakabe, Bull. Am. Phys. Soc. **61**, CP10.00059 (2016).

[44] D. A. Spong, R. Sanchez, and A. Weller, Phys. Plasmas **10**, 3217 (2003).

[45] H. L. Berk, J. W. Van Dam, D. Borba, J. Candy, G. T. A. Huysmans, and S. Sharapov, Phys. Plasmas **2**, 3401 (1995).

[46] B. N. Breizman, H. L. Berk, M. S. Pekker, S. D. Pinches, and S. E. Sharapov, Phys. Plasmas **10**, 3649 (2003).

[47] Y. Todo, K. Shinohara, M. Takechi, and M. Ishikawa, Phys. Plasmas **12**, 012503 (2005).

[48] X. D. Du, K. Toi, M. Osakabe, S. Ohdachi, T. Ido, K. Tanaka, M. Yokoyama, M. Yoshinuma, K. Ogawa, K. Y. Watanabe, M. Isobe, K. Nagaoka, T. Ozaki, S. Sakakibara, R. Seki, A. Shimizu, Y. Suzuki, and H. Tsuchiya (LHD Experiment Group), Phys. Rev. Lett. **114**, 155003 (2015).

[49] D. Wei, L. Yi, W. Xian-Qu, C. Wei, D. Yun-Bo, S. Ohdachi, J. Xiao-Quan, S. Yong, C. Jian-Yong, Z. Jun, F. Bei-Bing, L. Yong-Gao, H. Xian-Li, G. Jin-Ming, H. Xiao-Yu, H. Mei, and W. Xiao-Gang, Nucl. Fusion **54**, 013010 (2014).